Pure Appl. Geophys. 172 (2015), 699–718

DOI 10.1007/s00024-014-1012-7

Pure and Applied Geophysics

Observations and Numerical Modeling of the 2012 Haida Gwaii Tsunami off the Coast of British Columbia

Isaac V. Fine,[1] Josef Y. Cherniawsky,[1] Richard E. Thomson,[1] Alexander B. Rabinovich,[1,2] and Maxim V. Krassovski[1]

Abstract—A major (M_w 7.7) earthquake occurred on October 28, 2012 along the Queen Charlotte Fault Zone off the west coast of Haida Gwaii (formerly the Queen Charlotte Islands). The earthquake was the second strongest instrumentally recorded earthquake in Canadian history and generated the largest local tsunami ever recorded on the coast of British Columbia. A field survey on the Pacific side of Haida Gwaii revealed maximum runup heights of up to 7.6 m at sites sheltered from storm waves and 13 m in a small inlet that is less sheltered from storms (Leonard and Bednarski 2014). The tsunami was recorded by tide gauges along the coast of British Columbia, by open-ocean bottom pressure sensors of the NEPTUNE facility at Ocean Networks Canada's cabled observatory located seaward of southwestern Vancouver Island, and by several DART stations located in the northeast Pacific. The tsunami observations, in combination with rigorous numerical modeling, enabled us to determine the physical properties of this event and to correct the location of the tsunami source with respect to the initial geophysical estimates. The initial model results were used to specify sites of particular interest for post-tsunami field surveys on the coast of Moresby Island (Haida Gwaii), while field survey observations (Leonard and Bednarski 2014) were used, in turn, to verify the numerical simulations based on the corrected source region.

Key words: 2012 Haida Gwaii earthquake and tsunami, Northeast Pacific bottom pressure records, NOAA DART, Ocean Networks Canada (NEPTUNE facility), Tide gauge measurements, Numerical modeling.

1. Introduction

At 03:04 UTC on October 28, 2012, a major (M_w 7.7) earthquake occurred off the west coast of Moresby Island located at the southern end of Haida Gwaii (formerly the Queen Charlotte Islands). The earthquake caused several local landslides on Moresby Island (Southern Haida Gwaii) and minor damage in and near Queen Charlotte City on the eastern side of the island (James *et al*. 2013). The 2012 Haida Gwaii earthquake was the second strongest instrumentally recorded earthquake in Canadian history and the largest thrust earthquake ever recorded along this predominantly strike-slip margin (Cassidy *et al*. 2013; Nykolaishen *et al*. 2014). The Queen Charlotte Fault (QCF) Zone, along which the earthquake took place, constitutes a transform boundary between the Pacific and North American plates (Barrie *et al*. 2013). The boundary extends over 350 km along the western margin of British Columbia offshore of the Haida Gwaii archipelago (Fig. 1). In general, the QCF represents a complex and poorly understood transition, from the subduction of the oceanic plate beneath North America along the Cascadia margin to a right-slip transform fault separating the Pacific and North American plates (Barrie *et al*. 2013). The 2012 Haida Gwaii earthquake generated a tsunami that strongly affected the nearby coast of Moresby Island and was widely recorded in the Pacific Ocean (cf. Leonard and Bednarski 2014; Lay *et al*. 2013). The West Coast/Alaska Tsunami Warning Center issued a warning for the area extending from the north coast of Vancouver Island to the Alaska-British Columbia border. The warning was cancelled 3 h after the earthquake when it became clear that there was no threat to local settlements in the area.

About two dozen major earthquakes with $M \geq 6.0$ have occurred in the region of the QCF

[1] Ocean Sciences Division, Department of Fisheries and Oceans, Institute of Ocean Sciences, 9860 West Saanich Road, Sidney, BC V8L 4B2, Canada. E-mail: Josef.Cherniawsky@dfo-mpo.gc.ca

[2] Russian Academy of Sciences, P. P. Shirshov Institute of Oceanology, 36 Nakhimovsky Prosp, Moscow 117997, Russia.

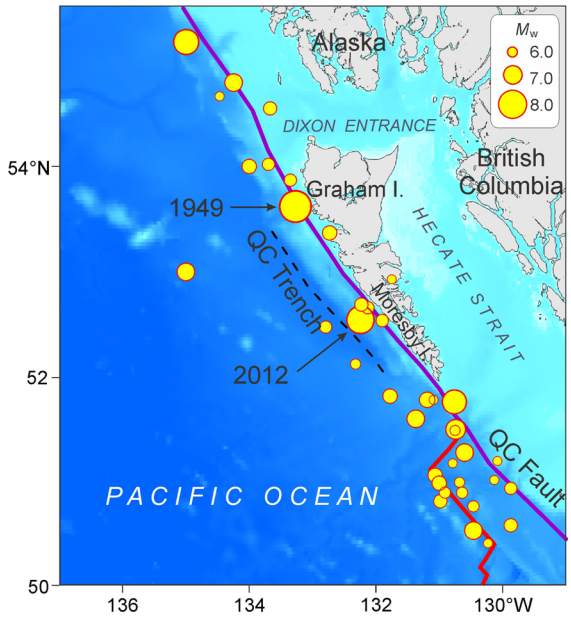

Figure 1
Epicenter locations and magnitudes of earthquakes of $M_w > 6.0$ in the Haida Gwaii region (formerly the Queen Charlotte Islands) during the last 100 years (Earthquake Canada 2014). *Circle* sizes are proportional to the earthquake magnitude (see legend); *QC* Queen Charlotte Trench and Fault

during the last century (Fig. 1), including the largest (M_w 8.1) earthquake of August 22, 1949. In contrast to the 2012 event, almost all of these earthquakes, including the 1949 event, had a strike-slip fault mechanism (Cassidy *et al.* 2010). Despite the considerable number of potentially tsunamigenic earthquakes in the area, there is very little information about tsunamis generated by QCF earthquakes. The 1949 tsunami was observed along the coast of southeastern Alaska and was instrumentally recorded at Sitka (maximum wave height of 7.5 cm) and at Hilo in the Hawaiian Islands ($\sim$10 cm) (Soloviev and Go 1975; Lander *et al.* 1993). This tsunami may have struck the coasts of Haida Gwaii and northern Vancouver Island, but there were no working tide gauges on these coasts at that time to substantiate this (Stephenson *et al.* 2007). A weak tsunami generated by the M_w 6.1 thrust fault earthquake off the coast of Haida Gwaii (Fig. 1) is discussed by Rabinovich *et al.* (2008) and Stephenson and Rabinovich (2009). The lack of information regarding historical tsunamis generated along the QCF zone can be attributed to the highly rugged and mostly unpopulated Pacific coast of Haida Gwaii. In addition, most earthquakes in the region have been of the strike-slip type, which are much less effective in generating tsunamis than thrust fault events (Ward 1980). The October 28, 2012 earthquake was one of the few thrust earthquakes in this region (Cassidy *et al.* 2013; Nykolaishen *et al.* 2014).

The 2012 Haida Gwaii tsunami propagated throughout the entire Pacific Ocean where it was recorded by numerous tide gauges on the coasts of the USA, Canada, Japan, New Zealand, and on various Pacific islands. The event was also recorded by a large number of open-ocean DART[1] stations off Alaska, the US West Coast, and other regions of the Pacific Ocean; the NOAA tsunami database contains references to more than 110 instrumental records of this event. The strongest far-field effects and the highest instrumentally recorded waves were observed on the Hawaiian Islands, thousands of kilometers from the source area (Lay *et al.* 2013). Moreover, the heights of the tsunami waves that struck Hawaii were of the same order of magnitude as those from much stronger earthquakes, such as the 2010 Chile and the 2006 Kuril Islands earthquakes. As revealed by the results of our numerical modeling (Sect. 3), Hawaii was positioned along the path of the main beam of offshore tsunami energy flux that was directed like a "searchlight" toward the islands (Fig. 2).

The present study focuses on the near-field characteristics of the 2012 tsunami for the coast of British Columbia (BC). It is near the source region in which the highest tsunami waves are expected to have occurred. Post-tsunami field surveys on the outer coast of Haida Gwaii revealed maximum runup heights in some sheltered bays of up to 7.6 m (Leonard and Bednarski 2014). The tsunami was also recorded by a number of coastal and offshore instruments in the Gulf of Alaska. We combine tsunami observations with numerical model simulations to obtain insight into the physical properties of this event as well as to test the accuracy of the tsunami source model derived using the inversion of the regional and global seismic time series from the earthquake (cf. Hayes 2013; Lay *et al.* 2013; Wei 2013; Shao and Ji 2013).

[1] *DART* deep-ocean assessment and reporting of tsunamis.

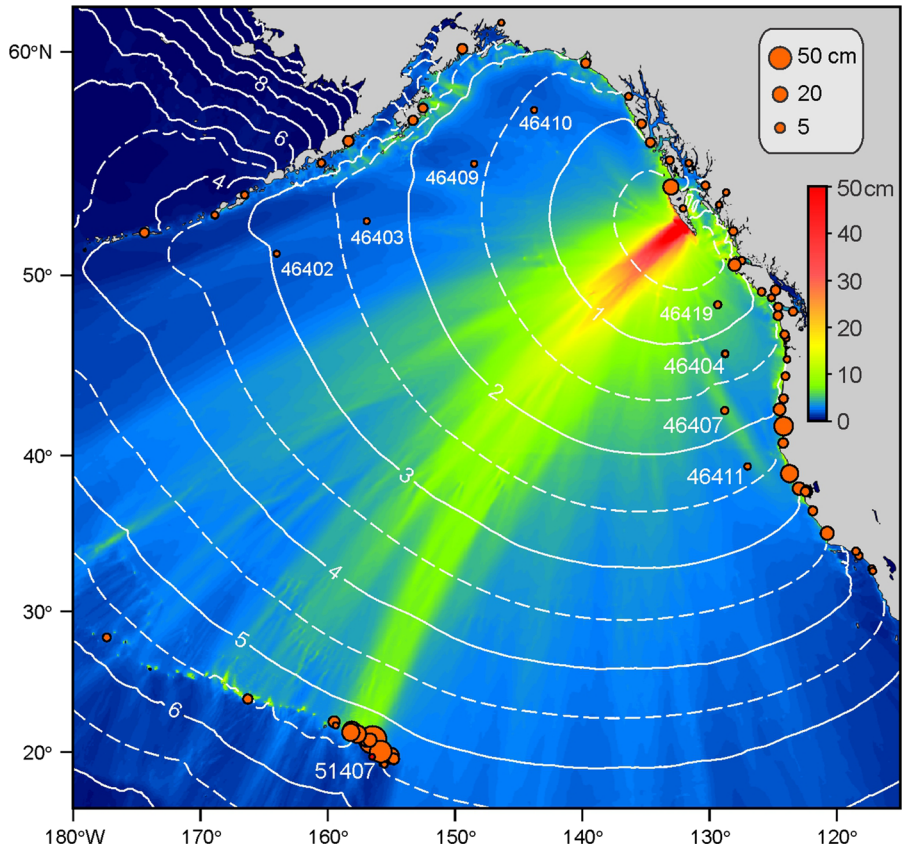

Figure 2
Maximum modeled tsunami elevations for the northeast Pacific. *Circles* denote the observed tsunami wave amplitudes at coastal tide gauges and deep-water stations. *White solid and dashed lines* are tsunami travel times (in hours)

2. *Observations*

The 2012 Haida Gwaii tsunami was measured in the northeast Pacific by a number of high-quality Canadian Hydrographic Service (CHS) digital coastal tide gauges, by NOAA DART stations, and by offshore bottom pressure recorders (BPRs) within the Canadian North-East Pacific Underwater Networked Experiments (NEPTUNE) component of the Ocean Networks Canada (ONC) cabled observatory array deployed to the west of Vancouver Island (Fig. 3).

2.1. *Observations for the British Columbia Coast*

Of the eleven BC coastal tide gauges (Table 1; Fig. 3) that recorded the 2012 Haida Gwaii tsunami, nine (Prince Rupert, Henslung Cove, Queen Charlotte City, Bella Bella, Port Hardy, Winter Harbour, Tofino, Port Alberni and Bamfield) are within the Permanent Water Level Network (PWLN) (Rabinovich and Stephenson 2004), and two (Hartley Bay and Kitimat) are temporary stations. The Victoria PWLN station was not operating during the event. Tide gauges located in the Strait of Georgia off the east coast of Vancouver Island (Fig. 3) showed no tsunami signal because they were effectively sheltered from the incoming tsunami waves.

To extract the tsunami wave signal from the time series, digital records from the BC coastal tide gauge stations were processed using data analysis procedures described by Rabinovich *et al*. (2006, 2008) and Stephenson and Rabinovich (2009). Specifically, we first removed the predicted tides from the data records and then high-pass filtered the residual (detided) time series using a 4-h Kaiser-Bessel (KB) window (cf. Thomson and Emery 2014) to suppress low-frequency sea level variations that are mainly associated with atmospheric processes. The tsunami

Figure 3
Map of coastal British Columbia showing the location of coastal tide gauges and open-ocean BPR stations that recorded the Haida Gwaii tsunami of October 28, 2012. The epicenter of the M_w 7.7 Haida Gwaii earthquake (Hayes 2013) is denoted by the *red star*. The *dashed brown line* indicates the seafloor NEPTUNE-Canada cable connecting BPRs with a coastal receiver at Port Alberni (P. Alberni). The abbreviated names of the Ocean Networks Canada (ONC) BPRs are: *CS* Clayoquot Slope, *BC* Barkley Canyon, *FP* Folger Passage, and *CORK* Circulation Obviation Retrofit Kit; the tide gauge QCC is at Queen Charlotte City. The *blue dashed lines* mark the 15-min isochrones (travel times of tsunami waves)

signal was clearly visible in all 11 records (Fig. 4). Table 1 presents the principal parameters of the observed tsunami waves.

Despite the substantial intensity of the earthquake and the relatively short distances of the recording sites from the source region, the tsunami waves observed at the BC tide gauge locations were remarkably small. As indicated in Sect. 3 (see also Lay *et al*. 2013), the maximum tsunami amplitude in the source area was about 2 m, while amplitudes recorded at the coastal tide gauges did not exceed 28 cm. (The maximum trough-to-crest wave height for the event was 53.5 cm recorded at Henslung Cove located on the southeastern coast of Langara Island, just north of Graham Island, Haida Gwaii). The relatively low amplitudes of the waves appear to be directly related to (1) the directivity of the tsunami source region, which generally parallels Moresby Island and which radiated the main tsunami energy in the offshore direction away from Haida Gwaii (Fig. 5), and (2) to the shadowing effect of Haida Gwaii, which protects the mainland coast of northern BC from direct wave impact (Figs. 3 and 5). To reach most of the tide gauges listed in Table 1, the tsunami waves traveled around the southern tip of Haida Gwaii. To reach Henslung Cove, the waves first propagated to the northwest along Haida Gwaii and then turned east around Graham Island, travelling through Dixon Entrance towards Prince Rupert and northern Hecate Strait (Figs. 3 and 5). Several salient features of the observed tsunami waves include the following:

- The waves were recorded along the entire exposed outer coast of BC and at several relatively protected inshore coastal stations, including Queen Charlotte City, Prince Rupert, Hartley Bay, Kitimat, and Port Hardy.
- Significant maximum tsunami heights were observed at Henslung Cove (53.5 cm), Winter Harbour (47 cm), and Port Alberni (43 cm), while considerably smaller waves were observed at other locations, ranging from 6 cm at Hartley Bay to 24 cm at Bella Bella. The first wave was positive (a crest) at all tide gauges except for Kitimat and Hartley Bay, which were shadowed from the main source by Moresby Island. For the two latter stations (which had the weakest tsunami records of all 11 tide gauge sites), the leading wave was negative (a trough). Based on the observed arrival times (Table 1), this trough wave cannot be directly linked to the tsunami wave originating from the main source area around Haida Gwaii, but may have originated with a weak secondary source area off the east coast of Moresby Island.
- The observed periods at most stations were between 20 and 35 min, except at Queen Charlotte City and Prince Rupert, where the periods were 9 and 105 min, respectively.

2.2. *Deep-Sea Observations*

Because they are not affected by coastal effects and have very low background noise compared to the shallow-water stations and coastal tide gauges, deep-

Table 1

Wave parameters of the Haida Gwaii tsunami of October 28, 2012 derived from tide gauge observations on the coast of British Columbia

Station	First wave			Maximum wave			Dominant wave period (min)
	Arrival (UTC)	Travel time[a]	Crest (+) or trough (−) (cm)	Maximum amplitude (cm)	Time (UTC) of max amplitude	Maximum height (cm)	
Bamfield	04:57	1 h 53 m	+6.5	6.5	05:02	13.3	23
Tofino	04:41	1 h 37 m	+7.5	11.6	07:32	20.6	25
Port Alberni	05:26	2 h 22 m	+19.2	22.3	08.21	42.7	33, 90
Winter Harbour	04:02	0 h 58 m	+15.6	22.2	07:48	47.1	35, 24
Port Hardy	04:43	1 h 39 m	+8.7	8.7	04:53	20.0	20–23
Bella Bella	04:29	1 h 25 m	+4.5	10.6	06:21	24.0	50
Queen Charlotte	05:44	2 h 40 m	+3.4	5.5	06:51	9.0	9
Henslung Cove	03:43	0 h 39 m	+14.5	27.2	04:58	53.5	22
Prince Rupert	05:01	1 h 57 m	+2.2	8.6	09:02	13.9	105
Hartley Bay	04:10	1 h 06 m	−2.9/+ 1.5	1.9	06:22	5.6	33
Kitimat	04:27	1 h 23 m	−2.3/+ 2.1	3.7	08:39	7.9	26

[a] The main (M_w 7.7) shock was at 03:04 UTC

water BPRs provide the most accurate and precise information about tsunami waves (cf. Titov *et al.* 2005; Thomson *et al.* 2011). The tsunami signals were recorded by the 9 NOAA DART stations in the northeast Pacific (Fig. 6), which switched into their 1-min event mode sampling at the time of the earthquake and then switched back to their usual 15-min sampling after several hours of event-mode sampling (see Mungov *et al.* 2013 for details of DART operations). Data from three of these stations, DART sites 46410, 46403, and 51407, were later recovered, providing both longer and higher quality (15-s) tsunami records. All DART records were de-tided. The four ONC BPRs located on the shelf, continental slope, and in deep water to the west of Vancouver Island (Fig. 3) had both the highest resolution (0.1 mm) and the highest sampling rate (1 s). Tsunami records from the ONC stations were de-tided, filtered with a 30-s Kaiser-Bessel (KB) low-pass filter (cf. Thomson and Emery 2014), and then re-sampled to 15-s intervals so that they were compatible with the rapidly-sampled mode of the DART records.

The tsunami records presented in Fig. 6 and Table 2 show spatial transformation of the tsunami signal over distances ranging from 430 km to more than 4,000 km from the source. In general, the recorded wave amplitudes were relatively small (<7 cm), primarily due to the fact that Station 51407 was sheltered from arriving tsunami waves by the Hawaiian Islands, while other observation sites were not in the main beam of the tsunami wave energy. All records reveal a leading wave crest, with waves at the southern DART stations having much higher amplitudes than equidistant northern DART stations. The southern DART stations also recorded steeper wave fronts and shorter periods for the leading wave. These features are mostly due to the anisotropy of the wave energy flux (Figs. 2, 5); the closer the station was to the main wave beam, the shorter the wave periods and the higher the wave amplitudes. For the DART records used in this study, lower amplitudes were observed at stations located closer to the shelf where waves propagating along the continental margin were leaking energy to waves trapped over the continental shelf (cf. Fine *et al.* 2013).

Some features of the tsunami waves are more clearly delineated by the ONC BPRs than by the DART BPRs. For example, the higher sampling rate by the ONC pressure recorders permitted detection and analysis of shorter waves. The ONC records show that the leading tsunami wave (with a period of ~35 min) was immediately followed by higher frequency wave trains with periods of about 3 min (Fig. 6b). Early arrival of these wave trains indicates that the short waves cannot be associated with the reflection but came directly from the source area.

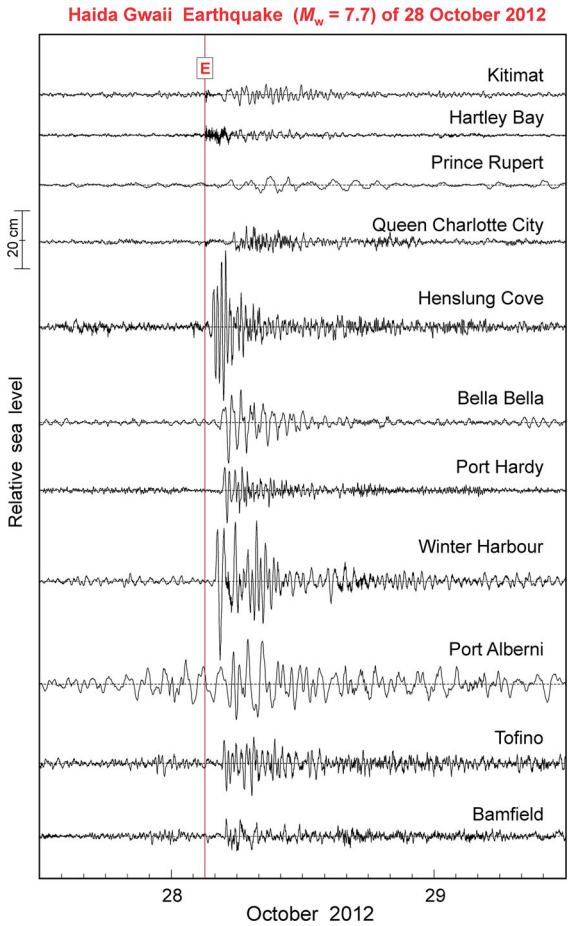

Figure 4
High-pass filtered sea level anomalies during the October 28, 2012 tsunami at 11 British Columbia coastal tide gauges. "E" denotes the time (UTC) of the earthquake

These short waves are not detectable in the DART records (Fig. 6a) because of insufficient temporal resolution of the time series. The much longer ONC records also reveal extensive "ringing" of the tsunami signal for up to three days as a result of the slow energy decay. We further note that the DART records in Fig. 6 contain strong seismically induced oscillations (primarily related to Rayleigh waves), which are almost imperceptible in the ONC 15-s records, except for a weak signal at CORK (the deepest of the four ONC stations).

It should be emphasized that the original 1-s ONC records had a prominent seismic wave signal with a range of more than 1.5 m and dominant periods of 8–9 s, but this signal was highly suppressed when we applied the 30-s low-pass KB filter and re-sampled the records to 15-s interval. In contrast, the 15-s boxcar window averaging applied to DART records to create 15-s samples (Meinig *et al*. 2005) does not effectively suppress the energetic seismic signal. As a consequence, the resulting signal was highly aliased by the seismic waves that "leaked" through the boxcar window, as evidenced by corresponding records in Fig. 6. [Thomson and Emery (2014) discuss the aliasing problem].

3. *Numerical Modeling: Fast-Track Results in Support of Post-Tsunami Field Surveys*

Within two weeks of the 2012 earthquake event, the first post-tsunami survey was organized by Natural Resources Canada, with participation from Fisheries and Oceans Canada (Leonard *et al*. 2012; Leonard and Bednarski 2014). The survey team required initial information on where to look for maximum tsunami wave heights on the west coast of Haida Gwaii. These estimates were provided by the "fast-track numerical model" (Fine *et al*. 2013).

The Fine *et al*. (2013) "fast-track" numerical tsunami model used in the present study is based on a finite-difference formulation of the linear shallow-water equations and is similar to that of Imamura (1996). We set up the numerical model for the following two distinct geographical domains: (1) A low-resolution northeast Pacific Ocean domain bounded by 15°–63°N, 180°–115°W, which was used for the far-field studies; and (2) a higher-resolution Haida Gwaii west coast domain which was used to simulate near-field tsunami waves and to guide the post-tsunami field surveys. For the far-field studies, the goal was to provide accurate estimates of the arrival times and initial tsunami waveforms at the remote deep-water stations. The latter requirements necessitate accurate simulation of tsunami wave frequency dispersion, which can be important for small source extension earthquakes (cf. González and Kulikov 1993). The classical approach is to use the Boussinesq-type wave equation (Chen *et al*. 2000). Other and less computationally demanding options include the use of a non-hydrostatic pressure correction term in the depth-integrated shallow-water equations

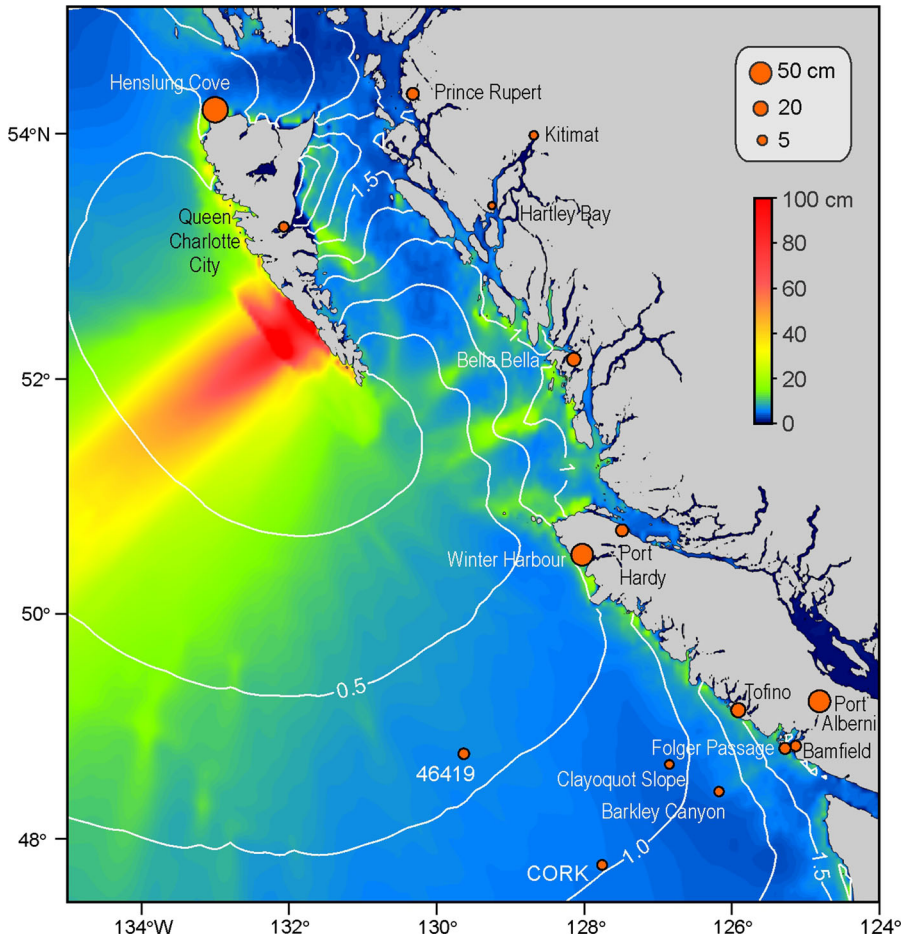

Figure 5
Maximum modeled tsunami elevations off the coast of British Columbia. *Orange circles* show the observed tsunami wave amplitudes at coastal tide gauges and deep-water stations. *White solid lines* mark the tsunami travel times (in hours)

(Kowalik 2012; Yamazaki *et al*. 2009), or mimicking physical dispersion with an equivalent numerical dispersion using the method of Imamura *et al*. (1988), later modified by Yoon (2002). Of the known methods, Imamura *et al*. (1988) is the most numerically efficient, which is why it is being used in many tsunami models (e.g., Titov *et al*. 2005; Nicolsky *et al*. 2011).

In the present study, we used Yoon's (2002) dispersion correction with the GEBCO bathymetry dataset (GEBCO 2013), degraded to three arc-min resolution in the north–south direction and four arc-min resolution in the west–east direction (~5.5 km). These values were chosen to keep the spatial resolution as high as possible while including the dispersion correction. To estimate the deformational shape of the bottom source, we used the finite-fault model of Hayes (2013). We found that this model produced a better tsunami source function for the 2012 Haida Gwaii earthquake than other available finite-fault models, specifically those by Shao and Ji (2013) and Wei (2013). The latter two models placed the source too close to Moresby Island, and this is why the simulated tsunami waves did not match the deep-ocean data.

The Hayes (2013) model provides the solution for a subducting plane with the following parameters: strike along 323.0° True, with a dip of 25.0°; seismic moment of 7.46×10^{20} Nm; and an earthquake hypocenter location at 132.101°W, 52.788°N, at a depth of 14 km. The Hayes' distribution function shows that most of the energy was released in the

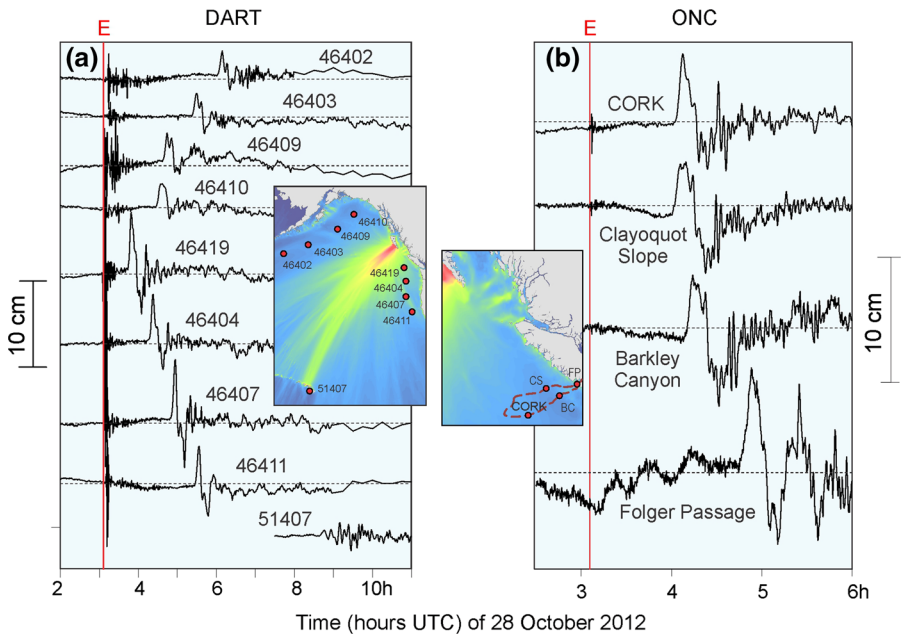

Figure 6
Observed records of the 2012 Haida Gwaii tsunami at **a** nine DART stations and **b** four ONC stations. "E" denotes the time of the earthquake. *Insets* show the instrument locations

Queen Charlotte Trench area (Figs. 1 and 7a). The original plate displacement data were recalculated into vertical bottom displacements using OKADA's (1985) equations and bathymetric data. Instead of applying the hydrostatic approximation, we used Laplace's equation and correction technique (FINE and KULIKOV 2011; FINE *et al.* 2013) to convert the resulting sea floor displacement into an initial sea surface displacement (Fig. 7b).

A comparison between the modeled tsunami waves and the observations at the four DART stations closest to the source region (46409 and 46410 to the north and 46404 and 46419 to the south; Fig. 2) shows that the modeled wave amplitudes and wave periods are in agreement with the observed values (Fig. 8a). However, the modeled arrival times deviate significantly from the observed arrival times. The frequency dispersion, which was partially taken into account, does not explain this mismatch because the signs of the time discrepancies are opposite for the northern and southern DARTs. In particular, the modeled waves arrived too early at the northern DART stations and too late at the southern stations.

To provide a quantitative measure of the agreement between the modeled (ζ_{mod}) and the observed (ζ_{obs}) sea level anomaly records, we used a skill number S defined as

$$S = 1 - \sum (\zeta_{obs} - \zeta_{\mathrm{mod}})^2 \Big/ \sum \zeta_{obs}^2 \qquad (1)$$

Except for Station 46409, the skill numbers for the DART stations, calculated for a 1-h time period, are relatively low (Fig. 8a). Late arrival of the simulated tsunami wave indicates that the actual location of the source differs from the initial location provided by HAYES (2013). This led us to the source correction analysis described in the next section.

4. Source Correction Based on the Deep-Ocean Tsunami Records

Estimates of the 2012 Haida Gwaii tsunami source location determined from seismological data can differ from the actual source region for several reasons. First, there were few nearby seismological stations to help constrain the source. Second, the

Table 2

Wave parameters of the Haida Gwaii tsunami of October 28, 2012, as recorded by DART stations and ONC bottom pressure recorders (BPRs)

Station name (depth in m)	First wave			Maximum wave			Dominant wave period (min)
	Arrival (UTC)	Travel time	Crest (+) or trough (−) (cm)	Maximum amplitude (cm)	Time (UTC) of max amplitude	Maximum height (cm)	
DARTs							
46419 (2775)	03:44	0 h 40 m	+6.7	6.7	03:49	11.9	23
46404 (2793)	04:15	1 h 11 m	+5.6	5.6	04:23	8.9	22
46407 (3322)	04:51	1 h 47 m	+7.0	7.0	04:57	12.9	23
46411 (4259)	05:28	2 h 24 m	+4.6	4.6	05:34	8.3	22
46410[a] (3782)	04:27	1 h 23 m	+2.75	2.75	04:34	4.2	26
46409 (4200)	04:38	1 h 34 m	+3.3	3.3	04:44	5.1	23
46403[a] (4512)	05:24	2 h 20 m	+2.7	2.7	05:29	4.9	24
46402 (4770)	06:02	2 h 58 m	+2.8	2.8	06:09	4.6	22
51407 (4738)	08:38	5 h 34 m	+0.7	1.5	09:10	3.3	10
ONC (NEPTUNE)							
CORK (2600)	04:02	0 h 58 m	+5.5	5.5	04:08	9.5	30
CS (1260)	04:01	0 h 57 m	+4.0	4.0	04:10	10.6	30
BC (410)	04:09	1 h 05 m	+4.9	4.9	04:14	11.0	30
FP (100)	04:45	1 h 41 m	+7.5	7.5	04:54	14.3	33

ONC stations are denoted by: *CS* Clayoquot Slope, *BC* Barkley Canyon, and *FP* Folger Passage

[a] DARTs 46403 and 46410 were retrieved from the bottom and a long series of 15-s data were downloaded; other DARTs had about 7 h of "event mode" data with a high sampling rate (15 s and 1 min) followed by the "standard mode" 15-min data

available stations had marked uncertainties in the regional seismic wave velocity values used to calculate travel times in the solid earth. Also, the wave "antenna" formed by the existing Natural Resources Canada seismic stations, located mainly along the coast of British Columbia, did not permit sufficiently precise estimation of the source area. It should be noted that the USGS (Hayes 2013) and Natural Resources Canada (Earthquakes Canada 2014) used somewhat different sets of seismic stations to define the earthquake deformation region, resulting in a difference of about 28 km in their derived epicenter locations.

One of the conventional methods to estimate the source boundaries and the exact location from the tsunami data involves the use of "inverse isochrones." In this method, the tsunami is assumed to originate at the observational points and travel backwards in time, with propagation beginning at the observed arrival times (cf. Fine *et al*. 2005; Hayashi *et al*. 2011). In the past, only coastal tide gauge data were available for this method. Consequently, regardless of the tide gauge location relative to the source region, the results often contained significant errors due to background noise, inaccuracies in the near-shore bathymetry, and in the tsunami arrival times. Because the deep-ocean records are much less susceptible to these problems, the observed arrival times for the deep sites can be estimated with much higher accuracy than for the coastal stations. In particular, faster propagation of the waves over the deep ocean makes the estimates less dependent on the quality and spatial resolution of the bathymetry data. (As an example, a tsunami wave moves 17 times faster in the 3,000-m deep ocean than in a 10-m deep coastal area.) Therefore, the resolution of the existing global bathymetry datasets, such as GEBCO, is more than adequate for accurate estimates of tsunami travel times in the deep ocean.

Based on the above discussion, we expect good agreement between the observed and computed arrival times for the deep-ocean stations. This, in turn, means that we can use the deep-ocean tsunami arrival and travel times (Table 2), together with the advanced tsunami travel time algorithm of Fine *et al*. (2013), to estimate the characteristics of the Haida Gwaii tsunami source region. A similar approach was used by Hayashi *et al.* (2011) to estimate the parameters of the 2011 Tohoku tsunami source based on the data from Japanese bottom cable stations. The

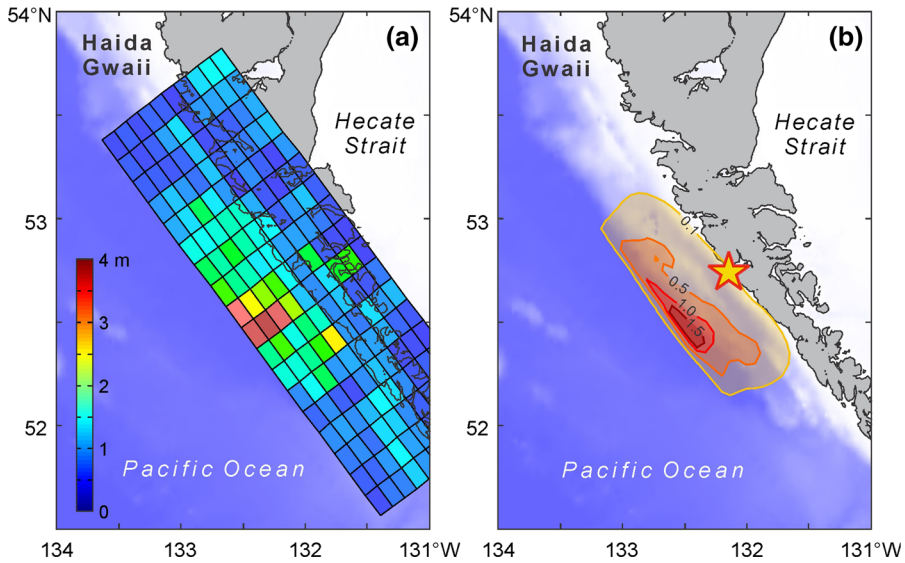

Figure 7

a Along-plate slip distribution from the HAYES (2013) finite fault model and **b** the computed initial sea surface elevation (in m) for the west coast of Haida Gwaii. The *yellow star* marks the earthquake epicenter according to the United States Geological Survey (USGS) (HAYES 2013)

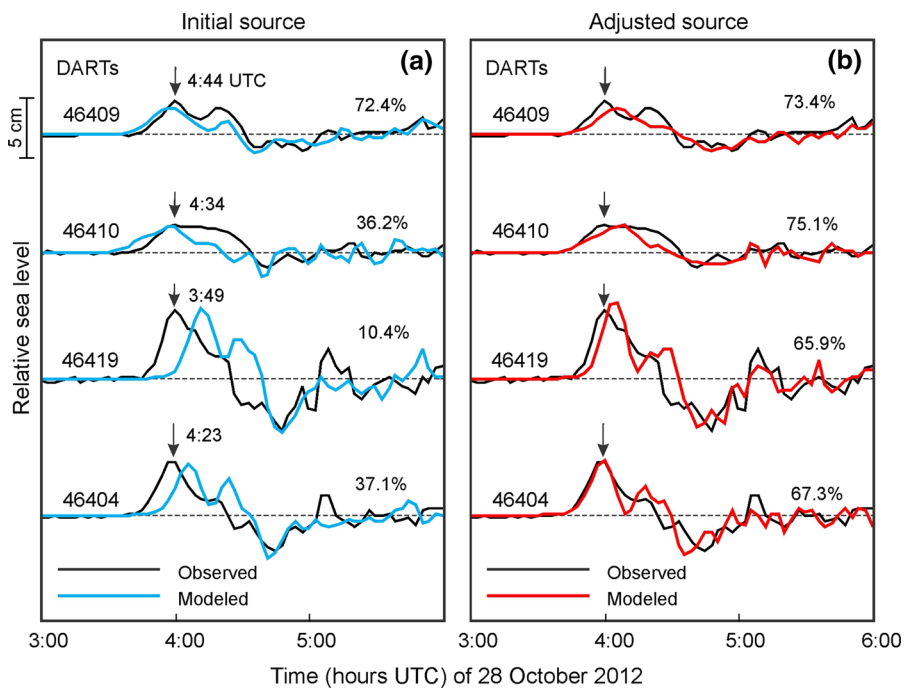

Figure 8

Comparison between the observed (*black lines*) and the modeled (*blue* and *red lines*) tsunami records at four DART stations closest to the tsunami source region; **a** results for the original source region provided by USGS; and **b** results for the shifted source region. The model skill numbers (in %) and the observed arrival times of the first crest maxima are shown for each station

results of our calculations for the four DART stations closest to the seismologically derived source region (two northern and two southern locations) show that the source was located off the west coast of Moresby Island in southern Haida Gwaii (Figs. 8b, 9). The inverse isochrones plotted for the observed travel times of the wave (thick solid lines in Fig. 9) encompass the estimated source area, while the isochrones for the observed travel times of the first crest maxima (dashed lines) define the rupture core zone. This is similar to the definition of the 2004 Sumatra tsunami source by FINE *et al.* (2005).

The spatial extent of the source region is similar to that obtained from the seismological data. However, our calculations indicate that the actual source was likely 25–35 km to the southeast of the seismically derived source region presented by HAYES (2013). The distribution of the aftershock ($M_w > 4.5$) locations (Fig. 9) agrees more closely with the source region obtained from the tsunami arrival times (ivory-colored area in Fig. 9) than with the original seismically-derived source region obtained by HAYES (2013) using the finite fault model (light magenta-shaded area). It is likely that the finite fault model had errors similar to those for the location of the earthquake epicenter as both were based on the initial USGS dataset and were not corrected with the local seismological data.

To estimate spatial shift in the source region that is needed to maximize the skill number, S (Eq. 1), for the four selected DART stations 46409, 46410, 46419, and 46404 (see insets in Fig. 6a for station location), we computed a 12 × 12 matrix of S values as a function of 12 incremental shifts in the zonal (x) and meridional (y) directions, using our numerical model for each of the 144 locations. The resulting distribution of S (Fig. 10), averaged for the above four DARTs, shows that the skill number increases (from 39.0 to 70.5 %) as the source region is shifted to the southeast (see Fig. 8a, b). Maximum skill is reached when the source is relocated 22 km to the south and 20 km to the east. This revised position of the source is used in our subsequent modeling of the Haida Gwaii tsunami.

To check the validity of the new position, we examined the agreement between the observed and modeled tsunami waves for four DART stations (46403, 46402, 46407 and 46411) and three ONC stations (CORK, CS, and Barkley Canyon) that had not been used to determine the correction for the source position. As illustrated in Figs. 11 and 12, the agreement between the observed and simulated tsunami records for both the DART and ONC stations is substantially improved upon correcting the source position, with the mean skill number for the DART stations increasing from 44.2 to 66.5 %, and that for the ONC stations from 38.4 to 63.7 %. The shifted position has also been confirmed by recent global positioning system (GPS) data analysis (NYKOLAISHEN *et al.* 2014).

The maximum tsunami elevation maps presented in Figs. 2 and 5 were obtained using the corrected source function. The numerical computations based on this function indicate that most of the tsunami energy was directed to the southwest, toward the Hawaiian Islands, which explains why the highest far-field tsunami amplitudes were recorded in that specific region (LAY *et al.* 2013). In general, the observed tsunami amplitudes along the Pacific coasts of the US and Canada are in good agreement with the simulated amplitudes. We have not presented a detailed comparison between the observed and modeled records at each coastal station since this would entail the use of models with nested grids and high-resolution bathymetry for each coastal location, leading to a major expansion in the scope of our study.

5. *Modeled Tsunami Waves for the West Cost of Haida Gwaii*

Our initial, "fast-track," tsunami model was run within two weeks after the earthquake to guide the first post-tsunami field surveys (LEONARD *et al.* 2012; LEONARD and BEDNARSKI 2014). The tsunami survey along the oceanic coast of Haida Gwaii proved very difficult as the region is highly inaccessible, sparsely populated, and strongly affected by storm-generated waves and swell (THOMSON 1981). The preliminary numerical estimates of the tsunami runup along the coast, which we provided with our model, turned out to be quite useful in planning the post-tsunami surveys because they helped the survey team concentrate

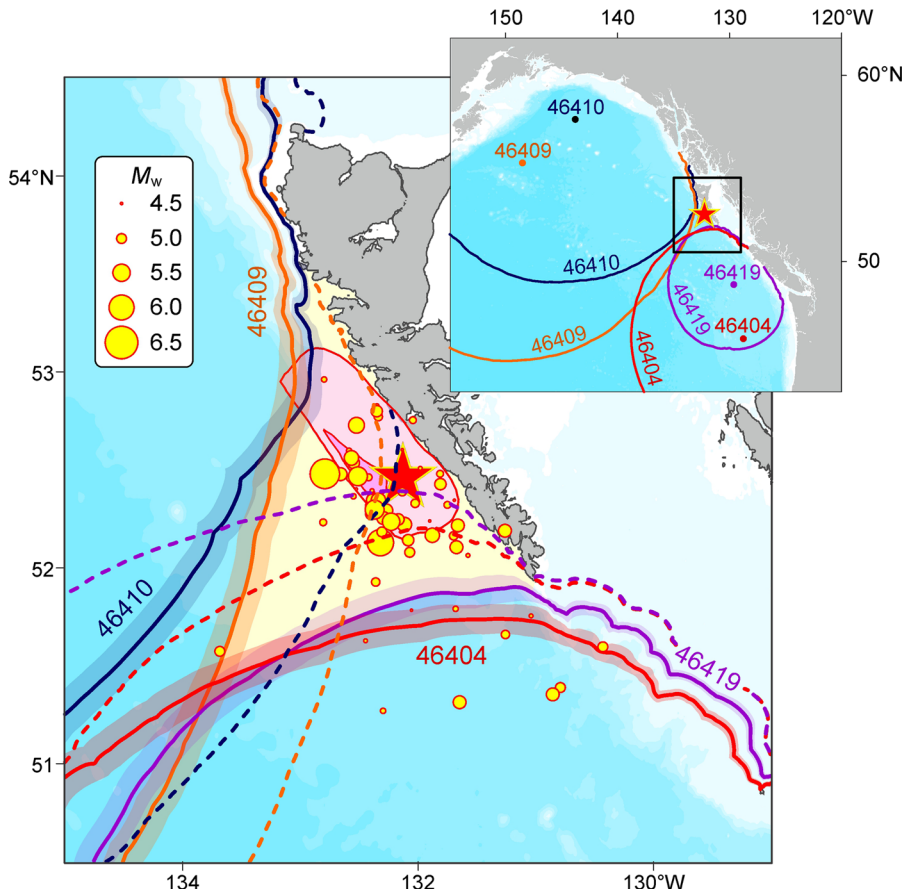

Figure 9

Inverse isochrones derived using the observed tsunami wave front travel times to the four nearest DART sites (*solid colour lines* with DART numbers) and the observed travel times of the first wave crest maxima (*dashed lines* of the same colour). The shading belts over frontal isochrones give estimates of the 1-min uncertainty in isochrone locations due to possible errors in bathymetry. The ivory area enclosed by the isochrones and the coastline indicates the expected position of the tsunami source estimated based on the DART observations. The *thin red lines* with *light magenta* shading areas are the 0.1- and 1-m contours of the initial sea surface displacement due to the original seismic source. *Yellow circles* show the aftershocks with magnitudes greater than 4.5 (Earthquakes Canada 2014). Bathymetry is shaded in blue. The inset shows the locations of the four DART instruments and the four inverse isochrones estimated from the respective tsunami observations

their effort on the areas of major interest (Leonard and Bednarski 2014).

As described in the previous section, the initial source function for the tsunami model was subsequently corrected, which led to much better agreement with the observations. To estimate the possible tsunami runup in the near-field zone located along the west coast of Moresby Island, we used a higher spatial resolution version of our numerical model. The near-field (regional) version of the model included nonlinear effects, which become important in the coastal zone, but excluded the less important frequency dispersion correction. The 147.6 × 134.9 km computational domain covered most of the west coast of Moresby Island along with the tsunami source region and surrounding areas (Fig. 13). To construct the digital bathymetry grid, we used high-resolution multi-beam and single-beam data provided by the Canadian Hydrographic Service, as well as the 30-arc s GEBCO data for the deep-water area. The grid had a spatial resolution of 50 m; this grid was used to estimate maximum tsunami wave heights along the coast. However, such relatively coarse resolution and lack of high-quality coastal topography data did not allow us to numerically simulate the tsunami runup and horizontal inshore inundation.

Figures 13 and 14 show the distributions of the computed water elevation maxima. As the modeling

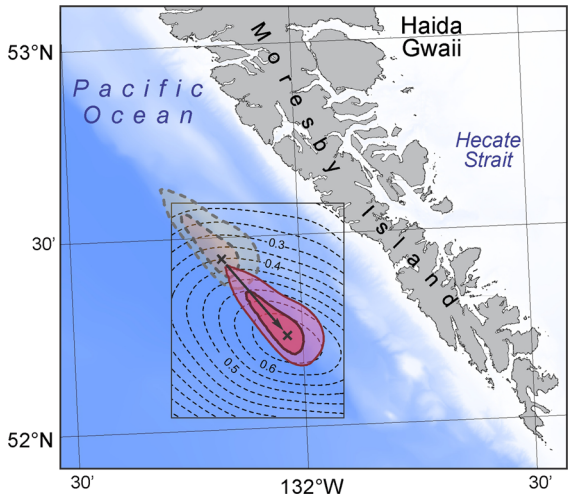

Figure 10
Spatial distribution of the averaged skill number (S) as a function of shifting the original source position in the zonal (x-shift) and meridional (y-shift) directions. The *thick arrow* shows the shift that yields the maximum skill number

demonstrates, the tsunami waves were highest along the west coast of Moresby Island, especially in the region between Tasu Sound and Gowgaia Bay, which lies directly to the northeast of the major seafloor displacement. The maximum amplitudes of the modeled waves in this area exceed 6 m, and, in some places, were close to 10 m. Due to the narrow shelf off the west coast of Moresby Island, there is little sustained "pumping" of tsunami wave energy from the deep ocean into the coastal region after the arrival of the first incident wave (Fine *et al*. 2013).

As noted in the Introduction and Sect. 2, there were no instrumental measurements of the tsunami on the west coast of Moresby Island. Although important information about the tsunami runup was obtained during the post-tsunami surveys in November 2012 and February and June 2013 (Leonard *et al*. 2012; Leonard and Bednarski 2014), the survey teams faced a number of challenges that limited their ability to obtain more extensive information. Among the challenges was a lack of eyewitness accounts, helicopter-only access to this remote and rugged coastline, and severe weather conditions at the time of the surveys. Moreover, because the outer coast of Moresby Island was hit by a severe storm on November 4, 2012, one week after the tsunami, the investigators only had confidence in their tsunami runup estimates inside the more sheltered bays and inlets.

To distinguish unquestionable tsunami debris from possible storm wave debris, Leonard and Bednarski (2014) separated the results from locations exposed to the storm waves from those protected from the storm impact. The first set of data shows generally higher runup values, although it is not clear if these are due to the tsunami runup or subsequent storm waves. A maximum runup of 13 m was found in the head of a small partly-sheltered inlet [2] located on the northern side of Tasu Sound. However, the most reliable runup height estimates were obtained in the more sheltered locations, where the signs of the abrupt sea level rise (such as seaweed hanging from tree branches) were obviously related to the tsunami waves. The highest runup values of up to 7.6 m were measured along the central part of the west coast of Moresby Island, between Tasu Sound and Gowgaia Bay; the runup values to the south and to the north of this area were lower. Indeed, the maximum tsunami heights from the model for this part of the coast are in relatively good agreement with the runup observations by the post-tsunami surveys (Fig. 14).

6. Discussion and Conclusions

The October 2012 tsunami was one of the highest tsunamis ever measured on the West Coast of Canada. The generated waves were of comparable height to those generated by the destructive 1964 event in Alaska (cf. Wigen and White 1964; White 1966). Equally importantly, the tsunami was generated by a local earthquake. This was the second strongest instrumentally recorded earthquake in Canadian history and the largest thrust fault earthquake ever observed along this predominantly strike-slip margin associated with the Queen Charlotte Fault Zone (Cassidy *et al*. 2013). The 2012–2013 tsunami field surveys (Leonard and Bednarski 2014) revealed that

[2] This uncharted inlet has no official name. It was called Davidson Inlet by Leonard and Bednarski (2014). An alternative name, Seaquake Inlet, was proposed by the Captain of the CCGS Bartlett, which carried out a custom bathymetric survey in this inlet on August 8, 2013. Given the observed large runup, the latter name may be quite appropriate.

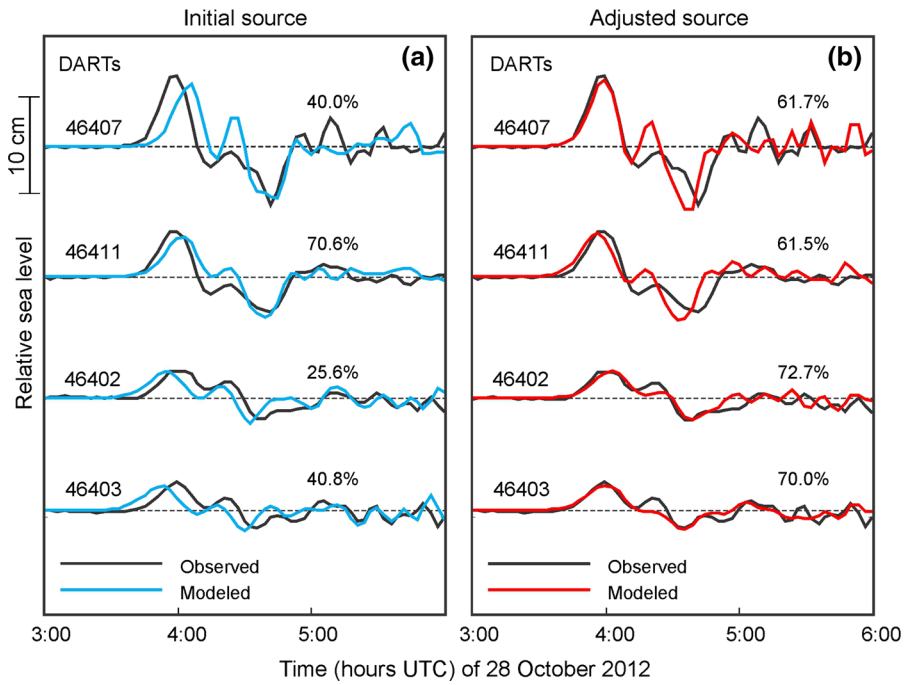

Figure 11
Comparison between the observed (*black lines*) and the modeled (*blue* and *red lines*) tsunami records at four DART stations; **a** results for the original source region provided by Hayes (2013); and **b** results for the shifted source region. The model skill numbers (in %) are shown for each station

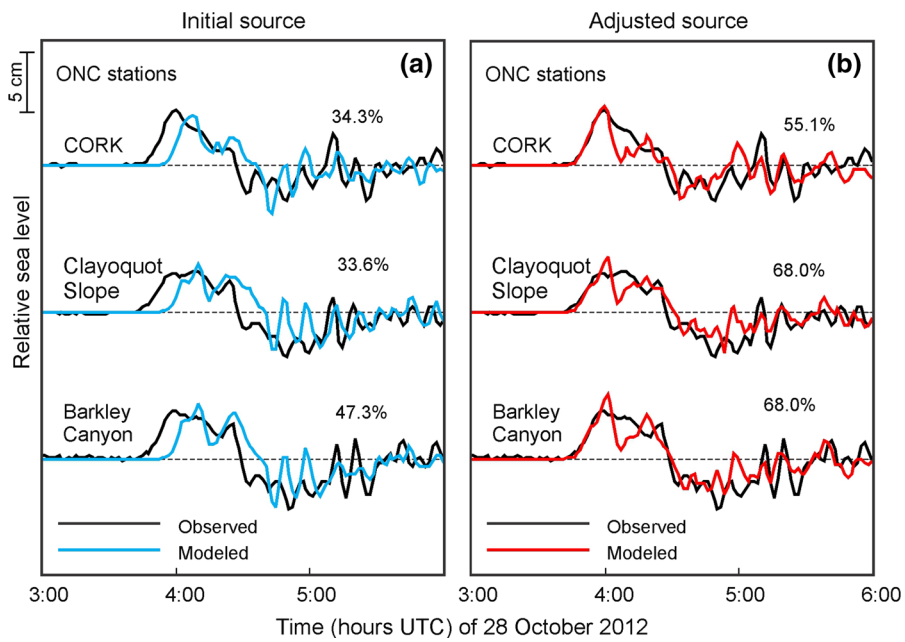

Figure 12
The same as in Fig. 11 but at three ONC stations

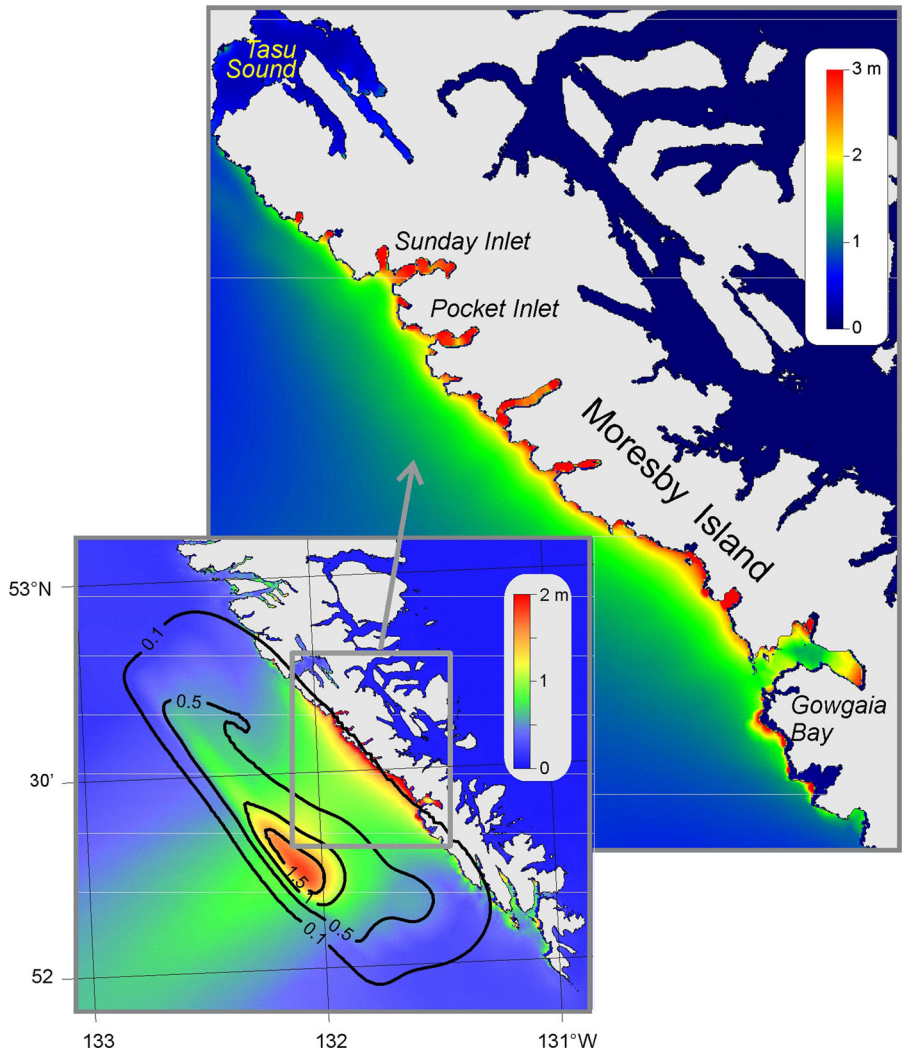

Figure 13
Maximum modeled tsunami elevations in the near-field zone. The inset also shows the contours of the initial sea surface uplift

much of the coastline of western Haida Gwaii was impacted by significant tsunami waves that probably reached 13 m above the state of tide,[3] while tsunami runup exceeding 3 m was observed at sites distributed along the 200 km long section of the coastline (Fig. 14). No one was injured by the tsunami as the area is highly remote and usually not populated during the stormy fall and winter periods. However, if a similar event were to occur during the summer, when more people visit the area, the risk would be much greater. This event clearly demonstrates a high tsunami risk associated with local major events for specific areas of the BC coast.

We were able to simulate the 2012 Haida Gwaii tsunami with a considerable degree of accuracy. In general, the principal factors that affect tsunami model reliability are the tsunami source distribution and the resolution of the near-shore bathymetry. In this study, we were partly able to address the first of these factors. To model the tsunami waves for the

[3] This large value is still under discussion as it was obtained on the coast of a partly exposed inlet which may have been affected by the destructive storm one week after the tsunami event. The maximum tsunami runup found by LEONARD and BEDNARSKI (2014) for the sheltered coastal areas was 7.6 m.

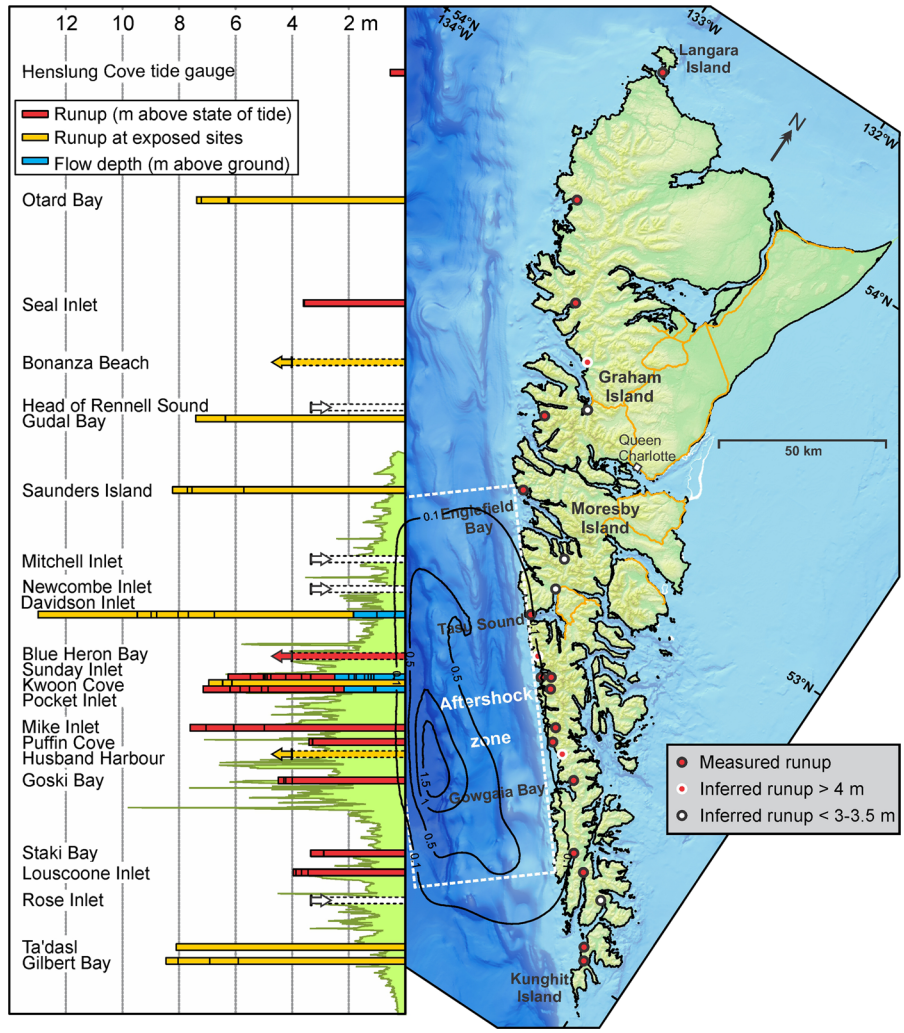

Figure 14

Maximum modeled tsunami elevations (*green line* with shading) and observed runup values (*red, yellow* and *white bars*) along the west coast of Moresby and Graham islands. The observed values are adapted from Leonard and Bednarski (2014). The *white dashed bars* give a maximum possible runup—i.e., as no debris was seen at elevations higher than the forest edge, runup cannot have been more than 3.5 m at these sheltered locations. The "inferred minimum runup"—*orange dashed bars* for exposed sites, *red dashed bars* at sheltered sites—was inferred by the observed presence of debris at elevations at least 1 m higher than the forest edge. With the forest edge no lower than 3 m above sea level (at the time of the tsunami), runup must have been no lower than 4 m. Also shown are the contours (*black lines*) of the tsunami source function and bathymetric relief in this area (*blue shading*)

northeast Pacific, we applied the seismological finite fault model of Hayes (2013) and the Okada (1985) formulation to define the original vertical displacement in the source region. The modeled amplitudes and periods of tsunami waves were in close agreement with those observed at the four open-ocean DART stations nearest to the source region (Fig. 8a). However, the modeled arrival times were markedly different from the observed arrival times, with the modeled waves arriving too early at the northern DARTs and too late at the southern DARTs. Using these DART records we show that the model results fit the data better (Fig. 8b) if the initial seismic source was shifted approximately 30 km to the southeast (Fig. 10). The modeled tsunami waves for the revised source position led to much better agreement with the

observed waves, including those recorded at DART and ONC stations that had not been used in the original fit analysis of the model (Figs. 11, 12).

It is interesting to compare the revised position of the source area, which is based on the HAYES (2013) model shifted to fit the DART data (Fig. 15a), with the sources constructed based on seismological information (Fig. 15b–d; cf. SULEIMANI *et al*. 2013). The sources of SHAO and JI (2013) (Fig. 15b) and WEI (2013) (Fig. 15d) are located too close to the shoreline of Moresby Island and disagree with the "revised Hayes source" (Fig. 15a). However, our source-corrected estimates have now been confirmed by NYKOLAISHEN *et al*. (2014), who recently corrected the source model of LAY *et al*. (2013) based on a reanalysis of GPS data. Their revised rupture zone (Fig. 15c) agrees well with our shifted tsunami source area based on the analysis of DART data (Fig. 10).

It should be noted that the "revised Hayes source" model (Fig. 15a), as well as the other 2012 Haida Gwaii source models (Fig. 15b–d), are relatively smooth and do not include small-scale details of the source region. This may explain why our numerical model does not reproduce the shorter-period ($T \sim 3$ min) oscillations which are clearly seen in the ONC records (Fig. 12).

The results of our study once again demonstrate the critical role of open-ocean tsunami observations, in addition to seismological data, in constraining tsunami source regions. The use of tsunami waveforms in the deep ocean, when combined with seismological inversion and GPS observations, significantly improves the accuracy of tsunami source functions and numerical models (cf. WEI *et al*. 2014; GUSMAN *et al.* 2014). We note, however, that we were not able to define the two-dimensional source region in sufficient detail based solely on the available remote BPR data, such that the boundaries of the tsunami source were maintained during the positional shift. On the other hand, the high skill values obtained for DART and ONC stations following the shift in the source position suggest that the shape of the tsunami source, which was constructed based on HAYES (2013) inversion of the seismic signals, was quite reasonable. While it is difficult to constrain the shape of the source using only BPR data, redefining the shape may be possible if data from seismic stations are also used. To simulate tsunami waves in real time, NOAA adopted a somewhat different approach, estimating the preliminary source using only seismic earthquake parameters. When additional tsunami records from DART buoys become available, their source is updated based on the DART time series of the event (cf. WEI *et al.* 2008; PERCIVAL *et al.* 2011; TANG *et al*. 2012).

Neither on-land seismic and GPS stations, nor the existing tsunami BPR network, can provide detailed distribution of the seafloor displacement in the source area. As a result, it has not been possible to map the source region of the 2012 Haida Gwaii tsunami with a high spatial resolution. This is unfortunate since information on the short-scale variations in the source region is needed for accurate modeling of tsunami wave propagation and runup in the near-field zone. In the case of the 2011 Tohoku tsunami, the runup data and numerous coastal and open-ocean instrumental records provided considerable information to constrain the spatial distribution and the small-scale details of the tsunami source function (cf. HAYASHI *et al.* 2011; SATAKE *et al.* 2013). For the 2012 Haida Gwaii tsunami, the only observations in the near-field zone were the data from the post-tsunami field surveys (LEONARD and BEDNARSKI 2014). Although very important for verification of the model results, these data were limited to a small number of sheltered bays and, therefore, were not sufficient to reconstruct the detailed shape of the tsunami source.

A serious shortcoming that impeded examination of tsunami waves in the Haida Gwaii region was the absence of local instrumental sea level measurements. The exposed and uninhabited shores of these islands create very serious problems for the installation of permanent tide gauge stations. As a result, there are no tide gauges on the west coast of Haida Gwaii resulting in a 540-km long gap between the CHS tide stations in Winter Harbour (northwest coast of Vancouver Island) and in Henslung Cove (Langara Island) (Fig. 3). In the absence of coastal sea level stations, the open-ocean DART measurements in this region would be especially important. Unfortunately, there are no operational deep-ocean instruments between DART 46410 and DART 46419 (Fig. 2), over a distance of about 1,360 km. This is the largest

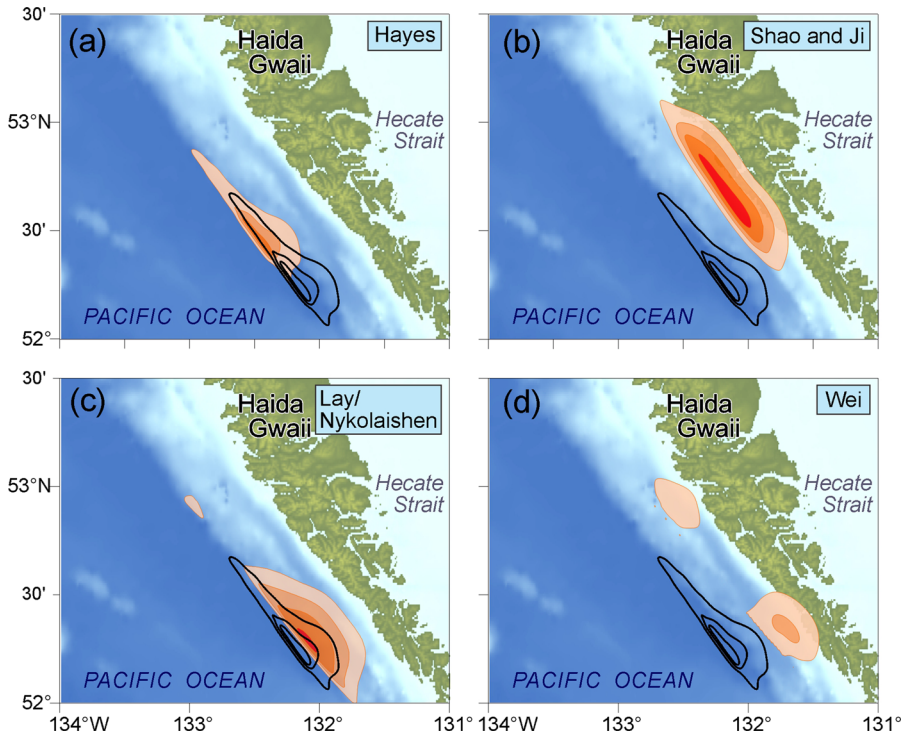

Figure 15
The 2012 Haida Gwaii tsunami sources: **a** Hayes (2013); **b** Shao and Ji (2013); **c** Lay *et al.* (2013), corrected by Nykolaishen *et al.* (2014); and **d** Wei (2013). *Black* contours show the "revised Hayes source" used in our model (contour intervals = 0.5 m)

gap in the tsunami monitoring system along the entire coast of North America. It was within the middle of this gap that the 2012 Haida Gwaii tsunami occurred (Fig. 2). This is quite different from the 2011 Tohoku tsunami, which was recorded by a great number of instruments located around the source area (cf. Satake *et al.* 2013).

Tsunami model results for the coastal zone also strongly depend on the availability and quality of the bathymetry data. While we have access to the high-resolution CHS bathymetric survey data, in some coastal areas these data are rather sparse or missing altogether. Our regional modeling results could, therefore, provide only approximate estimates of the 2012 Haida Gwaii tsunami maximum wave heights along the west coast of Moresby Island.

In conclusion, our numerical modeling study, which was initially designed to provide preliminary runup estimates for the west coast of Moresby Island as an aid to the post-tsunami survey team, indicates that, in many places along the coast, the simulated tsunami runup would have exceeded 6 m, which was confirmed by the subsequent field study. It is presently quite common to use tsunami field surveys to specify the source area and to verify numerical tsunami models. In our case, the post-tsunami survey and numerical simulation of tsunami waves worked in a coordinated manner, with the initial model helping to identify the sites of particular interest for the post-tsunami field surveys, followed by the use of the field observations (Leonard and Bednarski 2014) to verify the numerical model.

Acknowledgments

We are grateful to Lucinda Leonard and Jan Bednarski of the Pacific Geosciences Centre, Natural Resources Canada, for providing us with the latest results from their post-tsunami surveys; Elena Suleimani of the University of Alaska Fairbanks for her valuable comments; and to Peter Wills and personnel of the Canadian Hydrographic Service (CHS) for supplying us with the digital bathymetric data used to

construct the tsunami model grids. We thank Denny Sinnott (CHS) for the BC coastal sea level data used in this study. We also thank Yong Wei of the Pacific Marine Environmental Laboratory, Seattle, WA, and an anonymous reviewer for their useful comments and suggestions.

References

Barrie, J.V., Conway, K.W., and Harris, P.T. (2013), *The Queen Charlotte Fault, British Columbia: seafloor anatomy of a transform fault and its influence on sediment processes*, Geo-Marine Letters, *33*, 311–318, doi:10.1007/s00367-013-0333-3.

Cassidy, J.F., Rogers, G.C., Lamontagne, M., Halchuk, S., and Adams, J. (2010), *Canada's Earthquakes: 'The Good, the Bad, and the Ugly'*, Geoscience Canada, *37* (1), 1–16.

Cassidy, J.F. Rogers, G.C., and Hyndman, R.D. (2013), *An overview of the October 28, 2012 Mw 7.7 earthquake in Haida Gwaii, Canada: a tsunamigenic thrust event along a predominantly strike-slip margin*, Pure Appl. Geophys., *171*; doi:10.1007/s00024-014-0775-1.

Chen, Q., Kirby, J.T., Dalrymple, R.A., Kennedy, A.B., Chawla, A. (2000), *Boussinesq modeling of wave transformation, breaking and runup. II: two horizontal dimensions*. J. Waterway, Port, Coastal Ocean Eng., *126*, 48–56.

Earthquakes Canada (2014), *GSC, Earthquake Search (On-line Bulletin),* http://earthquakescanada.nrcan.gc.ca/stndon/NEDB-BNDS/bull-eng.php, Nat. Res. Can., last accessed on Nov. 27, 2014.

Fine, I.V., and Kulikov, E.A. (2011), *Calculation of the sea surface displacements within tsunami source area caused by instantaneous vertical deformation of seabed related to underwater earthquake*, Computational Technologies (Vychislitielnye Technologii) *16* (2), 111–118, (in Russian).

Fine, I.V., Rabinovich, A.B., and Thomson R.E. (2005), *The dual source region for the 2004 Sumatra tsunami*, Geophys. Res. Lett., *32*, L16602, doi:10.1029/2005GL023521.

Fine, I.V., Kulikov, E.A., and Cherniawsky, J.Y. (2013), *Japan's 2011 tsunami: Characteristics of wave propagation from observations and numerical modeling*, Pure Appl. Geophys., *170*, 1295–1307; doi:10.1007/s00024-012-0555-8.

González, F.I., and Kulikov, E.A. (1993), *Tsunami dispersion observed in the deep ocean*. In: *Tsunamis in the World* (Ed. S. Tinti), Kluwer Acad. Publ., Dordrecht. pp. 7–16.

Gusman, A.R., Tanioka, Y., MacInnes, B.T., and Tsushima, H. (2014), *A methodology for near-field tsunami inundation forecasting: application to the 2011 Tohoku tsunami*, J. Geophys. Res. - Solid Earth, doi:10.1002/2014JB010958 (in press).

Hayes, G. (2013), *Updated Finite Fault Results for the Oct 28, 2012 Mw 7.8 141 km S of Masset, Canada Earthquake (Version 2),* 2013, http://comcat.cr.usgs.gov/earthquakes/eventpage/pde20121028030408820_14#scientific_finite-fault, last accessed on Nov. 27, 2014.

Hayashi, Y., Tsushima, H., Hirata, K., Kimura, K., and Maeda, K. (2011), *Tsunami source area of the 2011 off the Pacific coast of Tohoku Earthquake determined from tsunami arrival times at offshore observation stations*, Earth, Planets Space, *63* (7), p. 809–813.

Imamura, F. (1996), *Review of tsunami simulation with a finite difference method*. In: *Long-Wave Run-up Models* (Eds. H. Yeh, P. Liu, and C. Synolakis), World Scientific, Singapore, pp. 25–42.

Imamura, F., Shuto, N., and Goto, C. (1988), *Numerical simulation of the transoceanic propagation of tsunamis,* Sixth Congress of the Asian and Pacific Regional Division, Int. Assoc. Hydraul. Res., Kyoto, Japan.

James, T., Rogers, G., Cassidy, J., Dragert, H., Hyndman, R., Leonard, L., Nikolayshen, L., Riedel, M. Schmidt, M., and Wang, K. (2013), *Field studies target 2012 Haida Gwaii Earthquake*, Eos, *94* (22), 197–198.

Kowalik (2012), *Introduction to Numerical Modeling of Tsunami Waves*, Fairbanks, 196 pp. (https://www.sfos.uaf.edu/directory/faculty/kowalik/Tsunami_Book/book_sum.pdf).

Lander, J.F., Lockridge, P.A., and Kozuch, M.J. (1993), *Tsunamis affecting the West Coast of the United States, 1806–1992*. Boulder, Colorado, National Geophysical Data Center, 242 pp.

Lay, T., Ye, L., Kanamori, H., Yamazaki, Y., Cheung, K.F., Kwong, K., and Koper, K.D. (2013). *Mw 7.8 Haida Gwaii underthrusting earthquake and tsunami: Slip partitioning along the Queen Charlotte Fault transpressional plate boundary*, Earth Planet. Science Lett., *375*, 57–70.

Leonard, L., Bednarski, J., Fine, I., Cherniawsky, J., and Wright, C. (2012), *The Haida Gwaii tsunami of October 27, 2012*, Risky Ground, Newsl. Centre for Natural Hazard Research, Simon Fraser University, Dec 21, 2012—Winter edn, 10–11, http://www.sfu.ca/cnhr/newsletters/RiskyGround_News_2012-12-21.pdf.

Leonard, L.J., and Bednarski, J.M. (2014), *Field survey following the 27 October 2012 Haida Gwaii tsunami*, Pure Appl. Geophys., *171*, doi:10.1007/s00024-014-0792-0.

Meinig, C., Stalin, S.E., Nakamura, A.I., and Milburn, H.B. (2005), *Real-Time Deep-Ocean Tsunami Measuring, Monitoring, and Reporting System: The NOAA DART II Description and Disclosure*, NOAA/PMEL, Seattle. 15 p.

Mungov, G., Eblé, M., and Bouchard, R. (2013), *DART® tsunameter retrospective and real-time data: A reflection on 10 years of processing in support of tsunami research and operations,* Pure Appl. Geophys., *170*, 1369–1384; doi:10.1007/s00024-012-0477-5.

Nicolsky, D.J., Suleimani, E., and Hansen, R. (2011), *Validation and verification of a numerical model for tsunami propagation and runup*. Pure Appl. Geophys., *168*, 1199–1222, doi:10.1007/s00024-010-0231-9.

Nykolaishen, L., Dragert, H., Wang, K., James, T.S., and Schmidt, M. (2014), *GPS observations of crustal deformation associated with the Mw 7.7 2012 Haida Gwaii earthquake*. Bull. Seism. Soc. Amer. (accepted).

Okada, Y. (1985), *Surface deformation due to shear and tensile faults in a half-space*, Bull. Seism. Soc. Amer., *75*, 1135–1154.

Percival, D.B., Denbo, D.W., Eble, M.C., Gica, E., Mofjeld, H.O., Spillane, M.C., Tang, L., and Titov V.V. (2011), *Extraction of tsunami source coefficients* via *inversion of DART® buoy data*, Natural Hazards, *58* (1), 567–590; doi:10.1007/s11069-010-9688-1.

Rabinovich, A.B. and Stephenson, F.E. (2004), *Longwave measurements for the coast of British Columbia and improvements to the tsunami warning capability*, Natural Hazards, *32* (3), 313–343.

Rabinovich, A.B., Thomson, R.E., and Stephenson, F.E. (2006), *The Sumatra Tsunami of 26 December 2004 as observed in the North Pacific and North Atlantic Oceans*, Surveys Geophys. *27*, 647–677.

Rabinovich, A.B., Thomson, R.E., Titov, V.V., Stephenson, F.E., and Rogers, G.C. (2008), *Locally generated tsunamis recorded on the coast of British Columbia*, Atmosphere-Ocean, *46* (3), 343–360.

Satake, K., Fujii, Y., Harada, T., and Namegaya, Y. (2013), *Time and space distribution of coseismic slip of the 2011 Tohoku earthquake as inferred from tsunami waveform data*, Bull. Seism. Soc. Amer., *103*, 1473–1492.

Shao, G., and Ji, C. (2013), *Preliminary Result of the Oct 28, 2012 Mw 7.7 Canada Earthquake* http://www.geol.ucsb.edu/faculty/ji/big_earthquakes/2012/10/canada.html, last accessed on Nov. 27, 2014.

Soloviev, S.L., and Go, Ch.N. (1975), *Catalogue of Tsunamis on the Eastern Shore of the Pacific Ocean*, Nauka, Moscow, 204 pp. [in Russian; English Translation: Canadian Transl. Fish. Aquatic Sci., No. 5078, Ottawa, 1984, 285 pp.].

Stephenson, F.E., and Rabinovich, A.B. (2009), *Tsunamis on the Pacific coast of Canada recorded in 1994–2007*, Pure Appl. Geophys., *166* (1/2), 177–210.

Stephenson, F.E., Rabinovich, A.B., Solovieva, O.N., Kulikov, E.A. and Yakovenko, O.I. (2007), *Catalogue of tsunamis, British Columbia, Canada: 1700–2007*. Preprint. P.P. Shirshov Inst. Oceanology, Moscow, 134 pp. (can be requested from the Institute of Ocean Sciences Library: http://www.dfo-mpo.gc.ca/libraries-bibliotheques/pac-reg-eng.htm).

Suleimani, E.N., Nicolsky, D.J., and Koehler, R.D. (2013), *Tsunami Inundation Maps of Sitka, Alaska*, Alaska Division of Geological & Geophysical Surveys Report of Investigation 2013-3, 76 p., 1 sheet, scale 1:250,000. doi: 10.14509/26671.

Tang, L., Titov, V.V., Bernard, E.N., Wei, Y., Chamberlin, C., Newman, J.C., Mofjeld, H., Arcas, D., Eblé, M., Moore, C., Uslu, B., Pells, C., Spillane, M.C., Wright, L.M., and Gica, E. (2012). *Direct energy estimation of the 2011 Japan tsunami using deep-ocean pressure measurements.* J. Geophys. Res., *117*, C08008, doi:10.1029/2011JC007635.

Thomson, R.E. (1981), *Oceanography of the British Columbia Coast*, Canadian Special Publication on Fisheries and Aquatic Sciences 56, Ottawa, 291 pp.

Thomson, R.E., and Emery, W.J. (2014), *Data Analysis Methods in Physical Oceanography*, Third Edition, Elsevier, New York, 716 pp.

Thomson, R.E., Fine, I.V., Rabinovich, A.B., Mihaly, S.F., Davis, E.E., Heesemann, M., and Krassovski, M.V. (2011), *Observations of the 2009 Samoa tsunami by the NEPTUNE-Canada cabled observatory: Test data for an operational regional tsunami forecast model*, Geophys. Res. Lett., *38*, L11701, doi:10.1029/2011GL046728.

Titov, V.V., González, F.I., Bernard, E.N., Eble, M.C., Mofjeld, H.O., Newman, J.C., and Venturato, A.J. (2005), *Real-time tsunami forecasting: Challenges and solutions*, Natural Hazards, *35* (1), Special Issue, U.S. National Tsunami Hazard Mitigation Program, 41–58.

Ward, S.N. (1980), *Relationships of tsunami generation and an earthquake source*, J. Phys. Earth, *28*, 441–474.

Wei S. (2013) *(Caltech, Masset 2012). Oct./28/2012 (Mw 7.8), Masset, Canada. Source Models of Large Earthquakes.* http://www.tectonics.caltech.edu/slip_history/2012_Masset/index.html, last accessed Nov. 27, 2014.

Wei, Y., Bernard, E., Tang, L., Weiss, R., Titov, V.V., Moore, C., Spillane, M., Hopkins, M., and Kânoğlu, U. (2008), *Real-time experimental forecast of the Peruvian tsunami of August 2007 for U.S. coastlines*, Geophys. Res. Lett., *35*, L04609, doi:10.1029/2007GL032250.

Wei, Y., Newman, A.V., Hayes, G.P., Titov, V.V., and Tang, L. (2014), *Tsunami forecast by joint inversion of real-time tsunami waveforms and seismic or GPS data: application to the Tohoku 2011 tsunami*. Pure and Appl. Geophys., *171* (12), doi:10.1007/s00024-014-0777-z.

White, W.R.H. (1966), *The Alaska Earthquake—its effect in Canada*, Can. Geogr. J., 210–219.

Wigen, S.O., and White, W.R.H. (1964), *Tsunami of March 27–29, 1964, West Coast of Canada*, Dept. Mines Techn. Surv., Victoria, BC, Canada, 12 pp.

Yamazaki, Y., Kowalik, Z., and Cheung, K.F. (2009), *Depth-integrated, non-hydrostatic model for wave breaking and run-up*, Int. J. Numer. Meth. Fluids, *61* (5), 473–497.

Yoon, S.B. (2002), *Propagation of distant tsunamis over slowly varying topography*, J. Geophys. Res., *107* (C10), 3140, doi:10.1029/2001JC000791.

(Received August 22, 2014, revised November 28, 2014, accepted December 8, 2014, Published online December 20, 2014)